PHYSICAL REVIEW D VOLUME 31, NUMBER 7 1 APRIL 1985

Production of composite neutral Higgs bosons in photoproduction and e^+e^- experiments

K. Whisnant and Bing-Lin Young
Department of Physics and Ames Laboratory, Iowa State University, Ames, Iowa 50011

Shike Hu
Department of Physics, Iowa State University, Ames, Iowa 50011
*and Department of Physics, Sichuan University, Chengdu, Sichuan, China**

(Received 12 November 1984)

We examine the consequences of a sizable tree-level coupling of a neutral Higgs boson to two photons, which could exist in composite models where the intermediate vector bosons and scalar Higgs bosons are made of the same subconstituents. We find that for certain ranges of the coupling strength and Higgs-boson mass, a neutral composite Higgs boson can be produced and detected in photon-proton scattering and e^+e^- annihilation at currently accessible energies. We also discuss other processes that are not present in the standard model at the tree level, but may lead to observable neutral-Higgs-boson production at, for instance, a $\bar{p}p$ collider.

I. INTRODUCTION

The Higgs particle, which is a crucial ingredient in the formulation of spontaneously broken gauge theories, turns out to be elusive, and perhaps experimentally inaccessible at the present if the minimal standard model is the final theory of electroweak interactions.[1] The difficulties in an experimental search for the Higgs particle are caused by the following facts.

(1) Except for some loose theoretical bounds, the mass of a Higgs boson is not known, making a systematic search for its existence difficult. Unitarity requires that m_H has an upper bound in the hundred of GeV range.[2] The lower bound,[3] which comes from the stability of the vacuum of the Higgs potential, requires that at least one of the Higgs bosons has a mass of no less than about 10 GeV.

(2) Its coupling to fermions is proportional to the ratio of the fermion mass and the weak-boson mass. This makes their production extremely improbable in the most common experimental situations with electron or ordinary hadron beams.

One strategy in dealing with the Higgs particle is to push its mass as high as allowed by the unitarity bound. The future generation of accelerator experiments will definitely be able to search for heavy Higgs bosons through its coupling to heavy quarks and the intermediate vector bosons. However, the possibility of the existence of not-so-heavy Higgs bosons should not be ignored. It is plausible, although not certain, that in the minimal standard model, in which only one scalar neutral Higgs boson exists, the Higgs boson is heavy, i.e., of the order of the weak-boson mass. In multi-Higgs-boson models, however, there are no compelling reasons for all the Higgs bosons to be heavy; in fact, some of the Higgs bosons, especially the scalar one, may well be light.[4]

Despite the observation of the Z^0 and $W^{\pm}$ bosons at their standard-model mass values,[5] it is very important that the spontaneous-symmetry-breakdown mechanism as given in the standard model is checked experimentally. To find the Higgs particle and to investigate its properties, or to establish its absence below the unitarity bound, will allow us to understand the real nature of the spontaneous symmetry breakdown of gauge theories. In fact, it may be more desirable to have the electroweak-gauge-symmetry-breakdown mechanism different from that in the standard model,[6] e.g., so that elementary scalar excitations could be eliminated. In a more general situation, Higgs-boson couplings may be different from those given in the standard model; couplings which are absent at the tree level in the standard model may or may not be suppressed in the general case. An example of this is the composite model in which Higgs bosons are composite states of certain fermion pairs.[7] In particular, it has been suggested recently that such a neutral Higgs boson may have a sizable coupling to two photons.[8] In the standard model the Higgs-boson—two-photon ($H^0\gamma\gamma$) coupling exists only through high-order processes and is therefore exceedingly small.

In this article we assume the possibility of a sizable $H^0\gamma\gamma$ coupling and investigate its effects in experiments which can be performed in the presently accessible energy regime. We find that in certain ranges of the $H^0\gamma\gamma$ coupling and Higgs-boson mass, H^0 can be produced and detected in several types of experiments.

In Sec. II, we review briefly the $H^0\gamma\gamma$ coupling in the composite models of Higgs particles and compare it with that in the standard model. We also discuss the Higgs-boson—Z^0—photon coupling. Sections III and IV discuss the production of an H^0 in the photoproduction and e^+e^- collision experiments. For photoproduction we concern ourselves with the energies available at the Fermilab and CERN photo-beam facilities and in e^+e^- collisions in the SLAC PEP and DESY PETRA energy regime. Possibilities at TRISTAN energies are discussed briefly at the end of Sec. IV. Production in other processes, such as $\bar{p}p$, are discussed in Sec. V, including the effect of the Higgs-boson—Z^0—photon coupling. A brief con-

clusion is given in Sec. VI. In the Appendix, we discuss some details of the three-photon signature of composite-H^0 production in e^+e^- annihilation not presented in the main text.

II. HIGGS-BOSON–TWO-PHOTON COUPLING

The $H^0\gamma\gamma$ coupling in the standard model exists only in high-order processes involving fermion and boson loops, and has been discussed in the literature. A summary will be given below. The process through a fermion loop[9] will be discussed first. For a pseudoscalar Higgs particle the loop diagrams are represented by convergent Feynman integrals, while for a scalar particle the integrals are superficially divergent. Dimensional[10] or Pauli-Villars[11] regularization will render the integrals finite and well defined. The decay width due to the fermion-loop contribution is[9]

$$\Gamma_f=\frac{\alpha^2}{4\pi^2}\frac{{m_H}^3}{4\pi}\sum_f\left|\frac{g_f}{m_f}{Q_f}^2 J_f\right|^2 , \tag{2.1}$$

where g_f is the $H^0f\bar{f}$ coupling constant. The summation runs over all contributing fermions f, Q_f is the electric charge of f in units of e, and J_f is an integral defined by

$$J_f\equiv\int_0^1 dx\int_0^{1-x}\frac{1-4xya}{1-R^2xy-i\epsilon}$$
$$=\frac{2a}{R^2}+\frac{(R^2-4a)}{R^4}\left[\mathrm{Sp}\left[\frac{2R}{R-(R^2-4)^{1/2}}\right]+\mathrm{Sp}\left[\frac{2R}{R+(R^2-4)^{1/2}}\right]^*\right], \tag{2.2}$$

where $a=1$ for scalar coupling, $a=0$ for pseudoscalar coupling, $R=m_H/m_f$, and Sp is the Spence function defined in Eq. (A10). Special properties of the Spence function[12] in this case allow evaluation of Eq. (2.2) in terms of elementary functions:

$$J_f=J_R+iJ_I , \tag{2.3a}$$

where

$$J_R=\begin{cases}\dfrac{2a}{R^2}+\dfrac{(R^2-4a)}{2R^4}\left[\pi^2-\ln\left[\dfrac{R}{2}[R+(R^2-4)^{1/2}]-1\right]^2\right], & R>2 ,\\ \dfrac{2a}{R^2}+\dfrac{2(R^2-4a)}{R^4}\left[\dfrac{\pi}{2}-\arctan\left[\dfrac{(4-R^2)^{1/2}}{R}\right]\right]^2, & R<2 ,\end{cases}$$
$$J_I=-2\pi\frac{(R^2-4a)}{R^4}\ln\left[\frac{R+(R^2-4)^{1/2}}{2}\right]\theta(R-2) . \tag{2.3b}$$

Note that in the minimal standard model g_f/m_f is independent of fermion species and can be factored out of the summation.

Another set of graphs is the boson-loop contributions, involving the intermediate vector bosons $W^\pm$ and possibly ghost fields. This class of diagrams has been evaluated in Ref. 13.

The total width of the H^0 into two photons in the standard model can be written as

$$\Gamma_{H\to\gamma\gamma}=\frac{\alpha^2}{8\sqrt{2}\pi^3}G_F{m_H}^3|I|^2 , \tag{2.4}$$

where

$$I=I_l+I_q+I_W , \tag{2.5a}$$
$$I_f=\sum_f {Q_f}^2 J_f , \tag{2.5b}$$
$$I_W=-\tfrac{7}{4} , \tag{2.5c}$$

where J_f is defined in Eq. (2.2) above. The lepton and quark contributions I_l and I_q are obtained from Eq. (2.5b) by summing over contributions from all the leptonic and quark intermediate states, respectively. The overall decay width of $\Gamma_{H\to\gamma\gamma}$ is plotted in Fig. 1 as a function of m_H. The partial widths of individual two-body channels in the standard model are listed in Table I for several values of Higgs-boson mass. The results will not be significantly modified in extended models of the electroweak interactions if there is a single origin of the masses of all the massive particles, as in the standard model. However, we do expect some modification of the entries in Table I for multi-Higgs-boson models where the leptons and quarks receive mass from different Higgs multiplets. Modifications will also be necessary if the gauge bosons and the fermions derive their masses from different Higgs multiplets.[4]

In a composite model in which the Higgs particle is a bound state of a fermion-antifermion pair, the $H^0\gamma\gamma$ coupling arises differently. Since the photon can couple to the subconstituents in a pointlike way, the $H^0\gamma\gamma$ coupling can be substantially larger than the standard model value. At the present time there exists a number of composite models characterized by different composite scales, from a few hundred GeV ($\sim {G_F}^{-1/2}$) to the Planck mass ($\sim 10^{19}$ GeV).[14] A unique prediction of the $H^0\gamma\gamma$ coupling, and therefore the rate for $H^0\to\gamma\gamma$, does not exist. However, models with low-mass compositeness scales are particularly interesting as they make predictions which allow tests of these models at the next generation of accelerators or even at available machines.[15] As sizable production rates of H^0 through its $\gamma\gamma$ couplings are possible

TABLE I. Partial widths for the leading two-body decay modes of a neutral Higgs boson. The gluonic and fermionic channels are calculated assuming standard-model couplings; the two-photon mode is calculated in the standard model (SM) and the two WDM scenarios. Partial widths are given in MeV, except for $\gamma\gamma$ (SM) which is in eV.

m_H (GeV)	gg	cc	$\tau\tau$	bb	$\gamma\gamma$ (I)	$\gamma\gamma$ (II)	$\gamma\gamma$ (SM)
5	0.0001	0.0038	0.0036		6.4	0.0051	0.29
10	0.0007	0.013	0.017	0.00	13.0	0.041	4.4
15	0.0023	0.021	0.029	0.10	19.0	0.14	16.0
20	0.0053	0.029	0.040	0.21	26.0	0.33	39.0
25	0.010	0.036	0.051	0.32	32.0	0.64	76.0
30	0.018	0.044	0.061	0.41	38.0	1.1	130.0

in some of the models,[8] existing accelerators might already produce Higgs bosons, especially with mass below 30 GeV. In any event, limits on the combined effects of the Higgs-boson mass and $H^0\gamma\gamma$ coupling strength can be readily established.

A particularly interesting scheme of the $H^0\gamma\gamma$ coupling is the W-dominance model (WDM), an analog to the vector-meson-dominance model which approximates QCD well for low-energy hadronic physics. This approach treats the electroweak interaction as an effective theory in the same manner as the vector-meson-dominance model, current algebra, flavor SU(3) symmetry, etc., in QCD. There exists a large amount of literature on the possibility that the standard model is actually an effective theory, starting with the work of Bjorken[16] and Hung and Sakurai.[17] See Ref. 18 for the current status of this approach and for additional references.

We shall use two models of $H^0\gamma\gamma$ coupling, proposed in Ref. 8, to illustrate the sensitivity of the $\gamma\gamma$ mode as a means to search for low-mass Higgs bosons (<30 GeV). The effective Lagrangian for $H^0\to\gamma\gamma$ can be written in the gauge-invariant forms

$$L_S = f_{H\gamma\gamma}\phi_H \tfrac{1}{4}F_{\mu\nu}F^{\mu\nu} ,$$
$$L_P = f_{H\gamma\gamma}\phi_H \tfrac{1}{8}\epsilon^{\mu\nu\lambda\rho}F_{\mu\nu}F_{\lambda\rho} , \tag{2.6}$$

for scalar and pseudoscalar H^0, respectively, where $F_{\mu\nu}$ is the electromagnetic field tensor and ϕ_H the Higgs field. The $H^0\gamma\gamma$ coupling $f_{H\gamma\gamma}$ and the $H^0\to\gamma\gamma$ partial width are related through the well-known formula

$$f_{H\gamma\gamma}{}^2 = \frac{64\pi}{m_H{}^3}\Gamma_{H\to\gamma\gamma} . \tag{2.7}$$

In the following these two coupling schemes[8,19] will be sketched.

(a) WDM I. The $H^0\gamma\gamma$ coupling is determined by the derivative of the H^0 wave function at the origin, where H^0 is considered as a nonrelativistic bound state of a fermion-antifermion pair. Then[8]

$$\Gamma_{H\to\gamma\gamma} = C\alpha m_H \sin^2\theta_W , \tag{2.8}$$

where θ_W is the Weinberg angle and C is of order unity ($C=\frac{1}{2}$ and $C=\frac{3}{4}$ for pseudoscalar and scalar Higgs particles, respectively). This scheme gives a rather large $\gamma\gamma$ width, e.g., $\Gamma_{H\to\gamma\gamma}=12.8$ MeV for a scalar Higgs particle of $m_H=10$ GeV.

(b) WDM II. This is a double WDM in which H^0 couples to two W^0's, each of which in turn couples directly to a photon. The model is similar to the vector-meson dominance of $\pi^0\to\gamma\gamma$, in which π^0 couples to the vector mesons ρ^0 and ω^0, and the ρ^0 and ω^0 turn into photons directly. Then

$$f_{H\gamma\gamma} = \sin^2\theta_W / m_W , \tag{2.9}$$

which gives a width of H into two photons of $\Gamma_{H\to\gamma\gamma}=41.2$ keV for $m_H=10$ GeV, $\sin\theta_W=0.233$, and $m_W=83$ GeV.

The examples given in models (a) and (b) above represent a wide variation of the $H^0\gamma\gamma$ coupling, and do not lead to a unique prediction. On the other hand, they represent a spectrum of subconstituent models which can be tested experimentally.

A more intuitive scheme is to argue that the $H^0\gamma\gamma$ coupling is proportional to the size of the composite, i.e., inversely proportional to the composite-mass scale Λ_{eff}. The $H^0\gamma\gamma$ coupling strength is given by

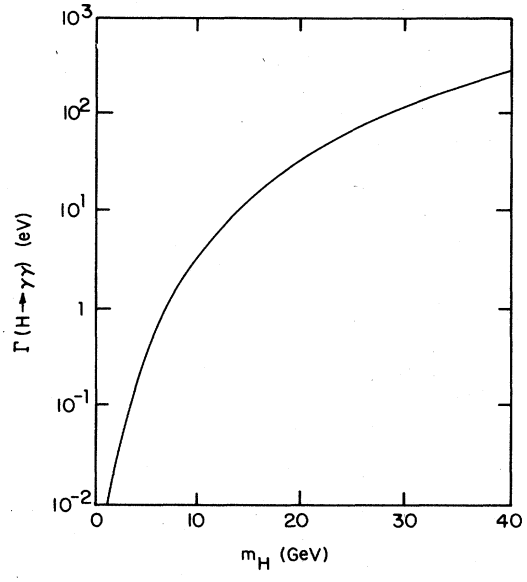

FIG. 1. Partial width for $H^0\to\gamma\gamma$ in the standard model versus Higgs-boson mass.

$$f_{H\gamma\gamma}=e^2/\Lambda_{\text{eff}} . \tag{2.10}$$

For a Higgs boson of mass 10 GeV, for instance, this leads to a decay width of $\Gamma_{H\to\gamma\gamma}=0.042$ keV for $\Lambda_{\text{eff}}=1$ TeV and $\Gamma_{H\to\gamma\gamma}=6.4$ keV for $\Lambda_{\text{eff}}=m_W$. The $\Gamma_{H\to\gamma\gamma}$ in the former case is similar to the standard model, and in the latter case is similar to case (b), WDM II. We will not consider this class of models as their predictions can be inferred from cases (a) and (b), once $f_{H\gamma\gamma}$ is given.

The couplings of Higgs bosons to fermion-antifermion pairs are expected to be the same in composite models as in the standard model in order to reproduce the quark and lepton mass spectra, and are therefore small for light fermions. Hence the partial widths of the fermion channels given in Table I are expected to be valid in composite models. Comparing the $\gamma\gamma$ width of the H^0 in composite models with the fermion-pair widths, we see that the $\gamma\gamma$ mode is dominant in WDM I and is no less than one-third of the total width in WDM II. However, this general feature has to be modified drastically if the subconstituents are colored objects. Then the Higgs boson would couple strongly to the two-gluon channel, which would dominate all other channels.[8] This is again in contrast to the case of an elementary Higgs boson, in which the Higgs-boson—gluon—gluon (Hgg) coupling arises solely through fermion loops,[20] and therefore is not overwhelmingly large.

Another coupling which does not exist at the tree level in the standard model, but may be present in composite models, is the $H^0Z^0\gamma$ coupling. In composite models, this coupling occurs through a simple electric (magnetic) dipole transition for a scalar (pseudoscalar) H^0, which is of the order of $f_{Hz\gamma}=\sin\theta_W/m_W$ using WDM.[8] It has the same gauge-invariant form as the $H^0\gamma\gamma$ coupling in Eq. (2.6). We discuss its effects in Secs. IV and V.

III. PHOTOPRODUCTION

Particles which have a sizable coupling to two photons can be produced in photoproduction experiments. The production mechanism is indicated in Fig. 2. For very light Higgs particles, say, $m_H<1$ GeV, and for elastic scattering off the target, the reaction is dominated by the well-known Primakoff effect.[21] In the present case, H^0 is probably not too light, so that the virtual photon exchanged with the target will be highly off mass shell. We shall assume a proton target and consider two cases: elastic and deep-inelastic scattering. It turns out that for both cases the differential cross section is suppressed with respect to electron-proton scattering by additional kinematic factors, and the photoproduction total cross sections in the two cases are comparable. Because of the proton form factor we expect that the production of a high-mass Higgs particle through proton elastic scattering will be suppressed in addition to the phase-space factor. On the other hand, we found that production of a heavy Higgs boson through deep-inelastic scattering is also suppressed because it occurs at high Feynman x. Both cross sections are strongly peaked in the forward direction, although it is more pronounced in elastic scattering because of the proton form factor.

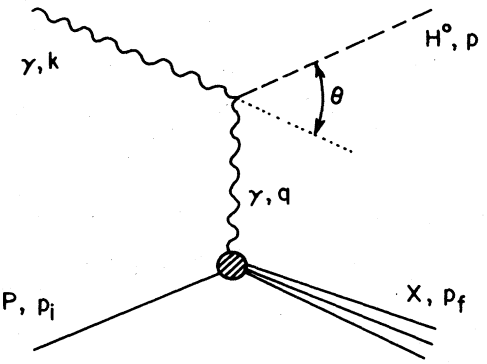

FIG. 2. Diagram for photoproduction of a composite neutral Higgs boson using a proton target.

A. Elastic scattering

Here X in Fig. 2 is a proton. The cross-section formula can be easily calculated. Using the notation of Gasiorowicz,[22]

$$\frac{d\sigma}{d\Omega_{\text{c.m.}}}=\frac{1}{256\pi^2 s}\frac{\lambda(s,m_p^2,m_H^2)}{\lambda(s,m_p^2,0)}\sum|A|^2 , \tag{3.1}$$

where the squared amplitude summed over spins is given by

$$\sum|A|^2=\frac{8\pi\alpha}{t^2}f_{H\gamma\gamma}^2\left[2[F_1(t)+\kappa F_2(t)]^2 t(k\cdot q)^2+\left[F_1^2(t)-\frac{t}{4m_p^2}\kappa^2F_2^2(t)\right][(k\cdot q)^2K^2+t^2(k\cdot K)]\right] . \tag{3.2}$$

We have used the definitions

$$q=k-p,\quad t=q^2,\quad K=p_i+p_f ,$$

$$\lambda(x,y,z)=(x^2+y^2+z^2-2xy-2xz-2yz)^{1/2}$$

and $\kappa=1.72$ is the proton anomalous magnetic moment in units of the Bohr magneton. The Dirac and Pauli form factors $F_1(t)$ and $F_2(t)$ are related to the electric and magnetic form factors $G_E(t)$ and $G_M(t)$ by

$$G_E(t)=F_1(t)+\frac{t}{4m_p^2}\kappa F_2(t) ,$$
$$G_M(t)=F_1(t)+\kappa F_2(t) , \tag{3.3}$$

which are generally parametrized by the dipole forms[23]

$$G_E(t)=\left[\frac{1}{1-t/0.71\ \text{GeV}^2}\right]^2 ,$$
$$G_M(t)=(1+\kappa)G_E(t) . \tag{3.4}$$

The results of the integrated total cross section are plotted in Fig. 3 as a function of the Higgs-boson mass for incident-photon energies of $E_\gamma = 100$ and 150 GeV in the laboratory frame. Note the increase in the cross section with larger photon energies. The maximum Higgs-boson mass that can be produced is constrained by kinematics to be

$$(m_H)_{\max} = (2E_\gamma m_p + m_p^2)^{1/2} - m_p \ , \tag{3.5}$$

which for $E_\gamma = 150$ GeV is about 16 GeV.

The signal to look for is either the Higgs-boson—two-photon decay mode or two-quark or two-gluon jets. As discussed in Sec. II, if the constituent fermions do not couple directly to gluons the two-photon mode of the H^0 will be significant, with a branching ratio of at least one-third. The two-photon mode would then offer the best possibility of looking for the neutral Higgs boson in photoproduction experiments. An additional attractive feature of this mode is that it allows a relatively accurate determination of the mass of the Higgs boson. However, if the constituent fermions couple strongly to the color gluons, the H^0 will decay almost exclusively into two-gluon jets, which again offers a clean signature provided that the recoil proton is tagged.

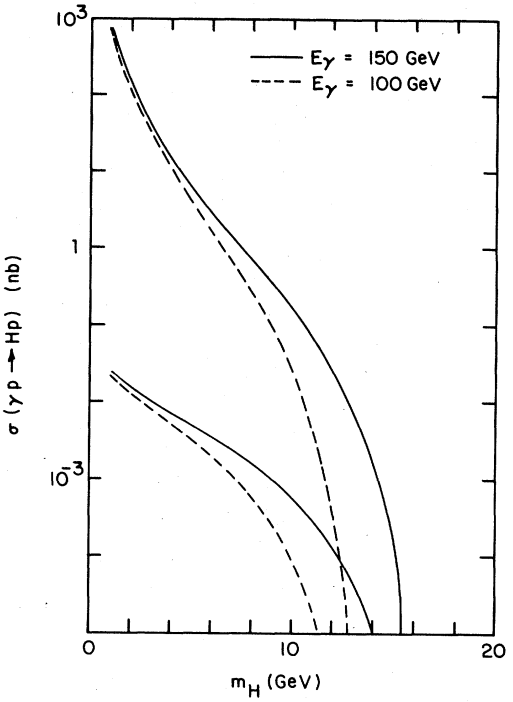

FIG. 3. Photoproduction cross section versus Higgs-boson mass for a composite neutral Higgs boson in elastic scattering off the proton for incident photon energies $E_\gamma = 100$ and 150 GeV. The upper and lower sets of curves are for WDM I and WDM II, respectively.

B. Deep-inelastic scattering

Here X in Fig. 2 can be anything. This is just normal deep-inelastic scattering as far as the proton target is concerned. We evaluate the cross section in the center of mass:

$$E_l \frac{d\sigma}{dm_X^2 \cos\theta_{\text{c.m.}}} = \frac{\alpha f_{H\gamma\gamma}{}^2 \lambda(s, m_X^2, m_H^2)}{64 s k_l m_p Q^4} \left[2(Q^2 + m_H^2)^2 W_1 + \left[4k_l^2 Q^2 - 2(Q^2 + m_H^2)\frac{k_l}{m_p}(m_X^2 + Q^2 - m_p^2) - (Q^2 + m_H^2)^2 \right] W_2 \right] , \tag{3.6a}$$

where k_l is the photon incident energy in the laboratory, $\theta_{\text{c.m.}}$ is the angle of the Higgs boson with respect to the incident photon in the center of mass, m_p is the proton mass, and $Q^2 = -q^2$. The integration ranges are

$$(m_p + m_\pi)^2 < m_X^2 < (\sqrt{s} - m_H)^2$$

and

$$-1 < \cos\theta_{\text{c.m.}} < 1 \ .$$

To compare with the usual e-p deep-inelastic scattering, Eq. (3.6a) can be written in terms of laboratory variables

$$E_l \frac{d^3\sigma}{dp_l^3} = \frac{\alpha f_{H\gamma\gamma}{}^2}{4\pi m_p k_l} \frac{k_l^2 p_l^2}{Q^2} \sin^2\left[\frac{\theta_l}{2}\right] \left[4\sin^2\left[\frac{\theta_l}{2}\right] W_1 + 2\cos^2\left[\frac{\theta_l}{2}\right] W_2 \right] \tag{3.6b}$$

in the limit $m_H \to 0$, where E_l and p_l are the energy and momentum of the Higgs particle and θ_l is the angle of the Higgs boson with respect to the incident photon direction in the laboratory. As alluded to before, Eq. (3.6b) differs from the lepton-scattering cross section by a factor $f_{H\gamma\gamma}{}^2 Q^2/32\pi\alpha$. (The same relationship also holds in the elastic case for $m_H \to 0$.) The familiar inelastic structure functions W_1 and W_2 are defined as

$$W_2(Q^2, x) \equiv \frac{m_p}{\nu} F_2(x) \ ,$$
$$W_1(Q^2, x) \equiv F_1(x) = \frac{1}{2x} F_2(x) \ , \tag{3.7}$$

where

$$m_p\nu \equiv p_i\cdot q \ , \qquad x\equiv\frac{Q^2}{q\cdot p_i} \ , \tag{3.8}$$

and

$$F_2(x)\equiv x[\tfrac{4}{9}u_v(x)+\tfrac{1}{9}d_v(x)+\tfrac{4}{3}s(x)] \ . \tag{3.9}$$

The proton distribution functions $u_v(x)$ and $d_v(x)$ are for the up and down valence quarks; $s(x)$ is the sea quark distribution function, assumed identical for up, down, and strange sea quarks. The contributions of heavy quarks are neglected. The explicit parametrizations of the quark distribution functions are taken from Ref. 24:

$$\begin{aligned} u_v(x)&=\frac{(1-x^2)^3}{\sqrt{x}}[0.594+0.461(1-x^2)^2 \\ &\quad +0.621(1-x^2)^4] \ , \\ d_v(x)&=\frac{(1-x^2)^3}{\sqrt{x}}[0.072+0.206(1-x^2)^2 \\ &\quad +0.621(1-x^2)^4] \ , \\ s(x)&=0.145x^{-1}(1-x)^9 \ . \end{aligned} \tag{3.10}$$

The parametrization of Ref. 25 gives almost identical results. The integrated cross sections for the deep-inelastic process are very similar to those for the elastic one shown in Fig. 3. The deep-inelastic cross sections tend to be nearly the same to 50% smaller than the elastic cross sections. There are two reasons for the difference. First, the elastic kinematic region extends to lower Q^2 where the cross section is the largest. Second, for large Higgs-boson-masses, while the elastic cross section is suppressed by the proton form factor, the inelastic Higgs-boson production occurs at large Feynman x, e.g., for $m_H=10$ GeV the average x value is about 0.7. This suggests that the search for H^0 in photoproduction experiments can best be performed with elastic scattering. The laboratory angle of the recoil proton can approach 45° when $m_H{}^2$ is small compared to s, which will help in its detection. Also, tagging a recoil proton in elastic scattering assures that a resonance, if produced, occurs at the photon vertex. Because the Higgs bosons are not seen directly, their production in the forward direction does not prohibit detection. However, difficulties may arise from the fact that the two-photon open angle may be small.

IV. e^+-e^- ANNIHILATION

Another possible production mechanism for a composite Higgs boson utilizing the $H^0\gamma\gamma$ vertex is[8] $e^+e^-\to\gamma^*\to H^0\gamma$. The differential cross section for this process, in the limit $m_e\to 0$, is

$$\frac{d\sigma}{d\cos\theta}=\frac{\alpha f_{H\gamma\gamma}{}^2}{64}\left[1-\frac{m_H{}^2}{s}\right]^3(1+\cos^2\theta) \ , \tag{4.1}$$

for either a scalar or pseudoscalar H^0, where θ is the angle of the H^0 with respect to the e^- beam in the laboratory frame. Using Eq. (2.6) to substitute for $f_{H\gamma\gamma}$, the total cross section is

$$\sigma=\frac{8\pi\alpha}{3}\frac{\Gamma_{H\to\gamma\gamma}}{m_H{}^3}\left[1-\frac{m_H{}^2}{s}\right]^3 \ . \tag{4.2}$$

The subsequent decay of the H^0 also depends strongly on the value of $f_{H\gamma\gamma}$ and the properties of its subconstituents, as discussed in the previous sections. If the subconstituents are colored objects, $H^0\to gg$ dominates, so that $e^+e^-\to\gamma+2$ gluon jets is more likely. Otherwise, $H^0\to\gamma\gamma$ will be a significant decay mode. Assuming that the H^0 couples to fermion proportional to their mass, as in the standard model, $H^0\to\gamma\gamma$ dominates in WDM I and is roughly equal to the leading $f\bar{f}$ modes in WDM II.

The $H^0\to\gamma\gamma$ decay gives a three-photon final state with one monochromatic direct photon of energy

$$E_\gamma=\frac{\sqrt{s}}{2}\left[1-\frac{m_H{}^2}{s}\right] \ , \tag{4.3}$$

and will provide a good way of detecting the H^0 if $B(H^0\to\gamma\gamma)$ is significant. The dominant background comes from QED production of two and three photons. Since the QED processes are strongly peaked along the beam, and the $H^0\gamma$ distribution is relatively flat, cuts can be made which eliminate much of the QED background. As a measure of this, we compare the $H^0\gamma$ and second-order QED $\gamma\gamma$ rates in the limit $m_e\to 0$,

$$\frac{d\sigma/d\Omega(e^+e^-\to\gamma\gamma\gamma)_{H\gamma}}{d\sigma/d\Omega(e^+e^-\to\gamma\gamma)_{\rm QED}}=\frac{s\Gamma_{H\to\gamma\gamma}}{2\alpha m_H{}^3}\left[1-\frac{m_H{}^2}{s}\right]^3\sin^2\theta \ . \tag{4.4}$$

For $m_H=10$ GeV and assuming WDM I (II), this ratio is about 60% (0.2%) at $\theta=90°$. Furthermore, if the H^0 is reasonably massive, the two photons from the H^0 will be distinct in their spatial positions, so that a requirement of three separated photons will further reduce the QED background.

Alternatively, the acollinearity distribution of the combined sample of two- and three-photon events can be used. This technique has been applied[26] in the experimental analysis of the pure QED processes $e^+e^-\to\gamma\gamma,\gamma\gamma\gamma$. The acollinearity angle is defined by

$$\zeta\equiv\arccos\left[\frac{\mathbf{p}_1\cdot\mathbf{p}_2}{|\mathbf{p}_1||\mathbf{p}_2|}\right] \ , \tag{4.5}$$

where $\mathbf{p}_1$ and $\mathbf{p}_2$ are the final-state photon three-momenta in the two-photon case, or the two most collinear final-state photon three-momenta in the three-photon case. For the pure QED process the acollinearity distribution is strongly peaked at $\zeta=0$, and falls to roughly 1% of the maximum value at $\zeta=0.2$.[26] The acollinearity distribution of the three-photon events from $H^0\gamma$ production depends critically on the H^0 mass compared to the available energy, and is shown in Fig. 4 for several values of $m_H/\sqrt{s}$ for WDM II. For $m_H{}^2\ll s$, the two photons from the H^0 decay are nearly collinear in the laboratory

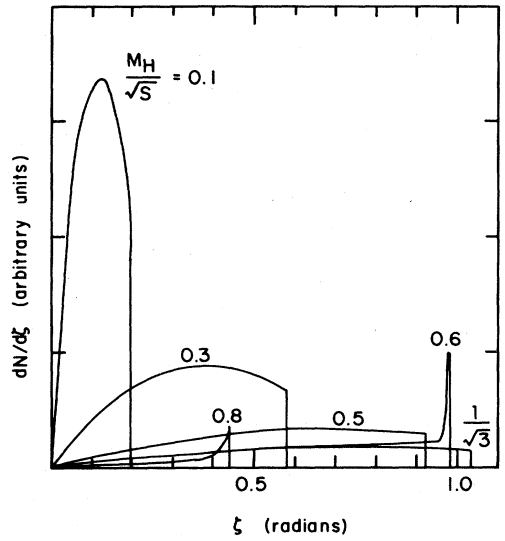

FIG. 4. Acollinearity distributions for the process $e^+e^-\to H^0\gamma\to\gamma\gamma\gamma$ for several values of $m_H/\sqrt{s}$. The relative normalization assumes WDM II.

frame, and therefore are nearly back-to-back with the direct photon, resulting in a strong peak near $\zeta=0$. For $m_H\approx\sqrt{s}$, the direct photon is very soft and the $H^0\to\gamma\gamma$ decay is nearly back-to-back in the laboratory frame, again producing a strong peak near $\zeta=0$. For values of m_H approaching $\sqrt{s}/\sqrt{3}$ from below there is a progressively flatter distribution which cuts off at

$$\zeta_{\max}\equiv\arccos\left[\frac{s-m_H^2}{s+m_H^2}\right]. \tag{4.6a}$$

At $m_H=\sqrt{s}/\sqrt{3}$, the distribution is the flattest and extends to maximum value $\zeta_{\max}=\pi/3$. For any value of m_H above $\sqrt{s}/\sqrt{3}$ but below $\sqrt{s}$, there is a sharp peak just below

$$\zeta_{\max}\equiv\arccos\left[\frac{8sm_H^2}{(s+m_H^2)^2}-1\right]. \tag{4.6b}$$

We note that for WDM II the shape of the distribution is completely determined by $m_H/\sqrt{s}$ and that the normalization depends only on the factor $(1-m_H^2/s)^3$. For WDM I the normalization is multiplied by a factor of $48\pi\alpha m_W^2/(\sin\theta_W m_H)^2$; otherwise there is no change from WDM II.

Simple detector cuts tend to skew the distribution to higher acollinearity. For instance, a common requirement is to have at least two photons be detected at more than a given minimum angle from the beam. It is clear that high-acollinearity, widely separated events are more likely to survive this cut than events which are nearly back-to-back. This may affect the position of the peak in the acollinearity distribution and hence the determination of the Higgs-boson mass by this method.

The above analysis is done in the narrow-width approximation; this is valid as long as the Higgs-boson width is very small compared to its mass. Exact formulas for non-negligible width and the details of the acollinearity analysis are presented in the Appendix.

At higher energies approaching the Z^0 mass, the $H^0Z^0\gamma$ vertex can contribute to H^0 production via the process $e^+e^-\to Z^0\to H^0\gamma$.[8] The differential cross section of Eq. (4.1) is then modified by the substitution

$$f_{H\gamma\gamma}{}^2\to f_{H\gamma\gamma}{}^2+\frac{-2vf_{H\gamma\gamma}f_{HZ\gamma}s(s-m_Z{}^2)+f_{HZ\gamma}{}^2(v^2+a^2)s^2}{(s-m_Z{}^2)^2+m_Z{}^2\Gamma_Z{}^2}, \tag{4.7}$$

where v and a are the vector and axial-vector coupling of the electron to the Z^0. Due to the small value of v, this correction is only about 1% at PETRA and PEP energies.

The above analysis can be extended to the TRISTAN energy region. Here the form factor effect in the $H^0\gamma\gamma$ coupling may not be negligible, as the virtual photon coupling to the e^+e^- initial state will be closer to the mass shell of the neutral vector bosons. Therefore the cross section formulas of Eqs. (4.1) and (4.2) have to be modified to include this affect. The form-factor effect here would enhance the production rate of H^0.

V. OTHER PROCESSES

Another consequence of the $Z^0H^0\gamma$ vertex is that the H^0 can appear in Z^0 decays for $m_H<m_Z$. The partial width for $Z^0\to H^0\gamma$ is

$$\Gamma(Z\to H^0\gamma)=\frac{f_{HZ\gamma}{}^2m_Z{}^3}{96\pi}\left[1-\frac{m_H{}^2}{m_Z{}^2}\right]^3. \tag{5.1}$$

Using the approximate partial decay rate to e^+e^- in the limit of vanishing electron-vector coupling to the Z^0,

$$\Gamma(Z^0\to e^+e^-)\approx\frac{\alpha m_Z}{48\sin^2\theta_W\cos^2\theta_W}, \tag{5.2}$$

valid for $\sin^2\theta_W\approx0.25$, we find

$$\frac{\Gamma(Z\to H^0\gamma)}{\Gamma(Z\to e^+e^-)}=\frac{f_{HZ\gamma}{}^2m_W{}^2\sin^2\theta_W}{2\pi\alpha}\left[1-\frac{m_H{}^2}{m_Z{}^2}\right]^3. \tag{5.3}$$

Thus, limits can be put on $f_{HZ\gamma}$ and m_H from $\bar{p}p$ collider data from the nonobservation of a hard photon. Assuming WDM, $f_{HZ\gamma}$ is expected to be $\sin\theta_W/m_W$,[8] in which case the ratio in Eq. (5.3) is of order unity as long as m_H is not too close to m_Z. We would not expect this mechanism to be the source of the anomalous $Z^0\to e^+e^-\gamma$ events[27] seen at the $\bar{p}p$ collider if the Higgs-boson coupling to fermion pairs is proportional to the fermion mass. The most likely signatures are $Z^0\to\gamma\gamma\gamma$, $Z^0\to f\bar{f}\gamma$, or $Z^0\to gg\gamma$ where f is the most massive fermion allowed by phase space. Potential limits on $f_{HZ\gamma}$ and m_H are shown in Fig. 5, assuming that the detection efficiencies for $H^0\gamma$ and e^+e^- decay modes are similar.

One well-known process for H^0 production in the standard model is the Wilczek mechanism,[20] the decay of a quark-antiquark bound state vector meson to H^0 and a photon, $V\to H^0\gamma$. This decay can also occur with composite Higgs bosons if the vector meson turns into a virtu-

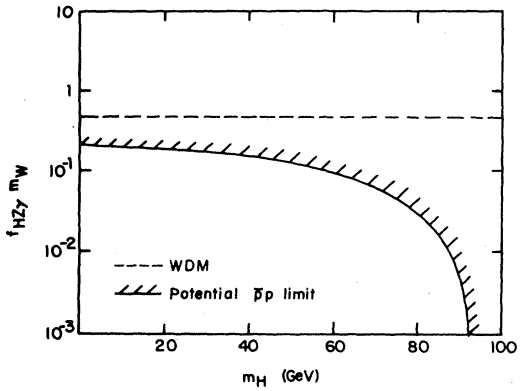

FIG. 5. Potential limits on the $H^0Z^0\gamma$ coupling in composite-Higgs-boson models from Z^0 production at a $p\bar{p}$ collider, assuming roughly equal detection efficiencies for $Z^0\to e^+e^-$ and $Z^0\to H^0\gamma$. The dashed line shows the WDM prediction.

al photon which then decays into $H^0+\gamma$, as shown in Fig. 6. The decay rate can be computed by the same method as the $V\to e^+e^-$ decay mode,[28] and gives

$$\frac{\Gamma(V\to\gamma^*\to H^0\gamma)}{\Gamma(V\to e^+e^-)}=\frac{f_{H\gamma\gamma}{}^2 m_V{}^2}{32\pi\alpha}\left[1-\frac{m_H{}^2}{m_V{}^2}\right]^3 . \quad (5.4)$$

As in the case for the Wilczek mechanism,[20] the prospect is better as the mass of the V state increases. Even for the Υ, however, $\Gamma(\Upsilon\to H^0\gamma)/\Gamma(\Upsilon\to e^+e^-)$ is of order 10^{-3} for composite Higgs bosons in WDM II even for $m_H \ll m_V$. For toponium at 80 GeV, for instance, the situation improves dramatically; we find

$$\Gamma(V(t\bar{t})\to H^0\gamma)/\Gamma(V(t\bar{t})\to e^+e^-)\sim 7\%$$

for $m_H \ll m_V$.

VI. DISCUSSION

We have considered in some detail the production of a light neutral Higgs boson with mass less than 16 GeV in photoproduction experiments, and in e^+e^- annihilation with $m_H < \sqrt{s}$. The property which is crucial to these experiments is the two-photon decay mode of the Higgs particle. In the standard model, minimal or extended, where Higgs particles are elementary field excitations, the $H^0\gamma\gamma$ coupling will be very small; the neutral Higgs boson, even if it were produced, could not be sorted out from the overwhelming number of background events. On the other hand, composite Higgs particles could have a sizable coupling to two photons. The experiments which have been suggested in this article are of conventional types and are accessible at the present time. Searches for the signals provided by the two-photon mode, or perhaps the two-gluon mode, will allow one to at least establish bounds involving m_H and $f_{H\gamma\gamma}$, and therefore set constraints on composite-Higgs-boson models.

In our discussion, we have ignored the possible form factor effects of the $H^0\gamma\gamma$ coupling for off-shell photons. Since the W bosons which dominate the photon channel are presumably heavy, of the order of 100 GeV, the variation in the four-momentum of the exchanged virtual photon in the photoproduction process will not be important. In the e^+e^- reaction the virtual photon is timelike, so that the form factor is expected to enhance the $H^0\gamma\gamma$ coupling. Nevertheless, in the energy range concerning us, the effect would be small. In the TRISTAN energy region, however, the form-factor effects become important, and must be taken into consideration.

ACKNOWLEDGMENTS

We would like to thank Jeff Appel and D. E. Wood for their many discussions concerning the experimental aspects of our work and for their continuing interest in the subject. We also appreciate the hospitality of W. A. Bardeen and H. B. Thacker during our visit to Fermilab, where a major portion of this work was completed. One of us (B.-L.Y.) would also like to thank H. Quinn for hospitality at SLAC where part of this work was performed. This work was supported by the U. S. Department of Energy under Contract No. W-7405-Eng-82, Office of Basic Science (KA-01-01), Division of High Energy Physics and Nuclear Physics.

APPENDIX

In this appendix we discuss the exact $e^+e^-\to\gamma\gamma\gamma$ cross section and distributions from the $H^0\gamma$ intermediate state, which arises from the diagrams shown in Fig. 7. The differential cross section is

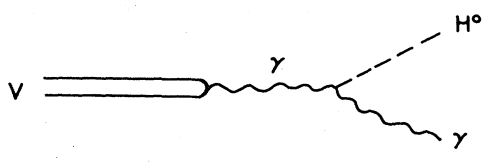

FIG. 6. Diagram for vector-meson decay $V^0\to H^0\gamma$ in composite-Higgs-boson models.

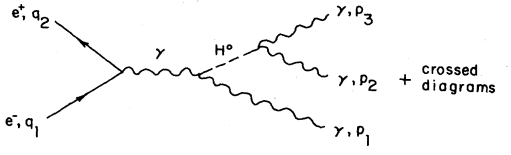

FIG. 7. Diagrams for the process $e^+e^-\to H^0\gamma\to\gamma\gamma\gamma$ in composite-Higgs-boson models.

$$\frac{d\sigma}{dx\,dy\,d\cos\theta\,d\beta}=\frac{2\alpha}{3\pi}\frac{\Gamma_{H\to\gamma\gamma}{}^2}{m_H{}^6}\left[\frac{4(p_2\cdot p_3)^2[(p_1\cdot Q)^2+(p_1\cdot P)^2]}{|D_{23}|^2}\right.$$
$$+2\,\mathrm{Re}\left[\frac{1}{D_{23}D_{13}}\right][(p_1\cdot Q)^2(p_2\cdot P)^2+(p_1\cdot P)^2(p_2\cdot Q)^2-2p_1\cdot p_3 p_2\cdot p_3 p_1\cdot P\,p_2\cdot P$$
$$\left.+4(p_1\cdot p_3)^2(p_2\cdot p_3)^2+sp_1\cdot Q\,p_2\cdot Q\,p_1\cdot p_2]+(1\leftrightarrow 2)+(1\leftrightarrow 3)\right], \tag{A1}$$

where $Q=q_1-q_2$, $P=q_1+q_2$, $D_{jk}=2p_j\cdot p_k-m_H{}^2+im_H\Gamma_H$, and x and y are defined as

$$x=\frac{2p_2\cdot p_3}{s},\quad y=\frac{2p_1\cdot p_3}{s}\ . \tag{A2}$$

The other vector products can be expressed in terms of x and y as

$$p_1\cdot P=\frac{s}{2}(1-x),\quad p_2\cdot P=\frac{s}{2}(1-y),\quad p_3\cdot P=\frac{s}{2}(x+y)\ ,$$
$$p_1\cdot Q=-\frac{s}{2}(1-x)(\cos\theta\cos\alpha+\sin\theta\sin\alpha\cos\beta)\ , \tag{A3}$$
$$p_2\cdot Q=-\frac{s}{2}(1-y)\cos\theta,\quad p_3\cdot Q=-(p_1-p_2)\cdot q\ ,$$
$$p_1\cdot p_2=\frac{s}{2}(1-x-y)\ .$$

Here θ is the angle of one of the photons with respect to the e^- beam, α and β are the polar and azimuthal angles, respectively, of a second photon with respect to the first; the angle α is determined by x and y,

$$\cos\alpha=\frac{xy+x+y-1}{(1-x)(1-y)}\ . \tag{A4}$$

The integration ranges are $0\le z\le 1$, $0\le y\le 1-x$, $0\le\beta\le 2\pi$, and $-1\le\cos\theta\le 1$. The azimuthal angle of the first photon has already been integrated. The remaining angular integrations are easily done; we find

$$\frac{d\sigma}{dx\,dy}=\frac{8\alpha}{9}\frac{\Gamma_{H\to\gamma\gamma}{}^2}{m_H{}^6}\left[\frac{x^2(1-x)^2}{D(x)}+\frac{y^2(1-y)^2}{D(y)}+\frac{(1-x-y)^2(x+y)^2}{D(1-x-y)}+\frac{N(y,1-x-y)y^2(1-x-y)^2}{D(y)D(1-x-y)}\right.$$
$$\left.+\frac{N(x,y)x^2y^2}{D(x)D(y)}+\frac{N(x,1-x-y)x^2(1-x-y)^2}{D(x)D(1-x-y)}\right], \tag{A5}$$

where we have made the definitions

$$N(x,y)=\left[x-\frac{m_H{}^2}{s}\right]\left[y-\frac{m_H{}^2}{s}\right]+\frac{m_H{}^2\Gamma_H{}^2}{s^2},\quad D(x)=N(x,x)\ . \tag{A6}$$

The first three terms in the large parentheses in Eq. (A5) are from the individual squared diagrams and the last three are interference terms. After a suitable change of variables the cross section can be reduced to

$$\sigma=\frac{8\alpha s}{3}\frac{\Gamma_{H\to\gamma\gamma}{}^2}{m_H{}^2}\left[I_1\left[\frac{m_H{}^2}{s},\frac{m_H\Gamma_H}{s}\right]+I_2\left[\frac{m_H{}^2}{s},\frac{m_H\Gamma_H}{s}\right]\right]. \tag{A7}$$

Defining $\mu = m_H^2/s$ and $a = m_H\Gamma_H/s$, the functions I_1 and I_2 are given by

$$I_1(\mu,a) = \int_0^1 dx \int_0^{1-x} dy \frac{x^2(1-x)^2}{D(x)}$$
$$= \tfrac{1}{4} - \tfrac{11}{3}\mu + \tfrac{15}{2}\mu^2 - 4\mu^3 - \tfrac{5}{2}a^2 + 4\mu a^2 + \tfrac{1}{2}(2\mu - 9\mu^2 + 12\mu^3 - 5\mu^4 + 3a^2 - 12\mu a^2 + 10\mu^2 a^2 - a^4)\ln\left[\frac{(1-\mu)^2+a^2}{\mu^2+a^2}\right]$$
$$+ \frac{1}{a}[\mu^2(1-\mu)^3 + 9\mu a^2 - 18\mu^2 a^2 + 10\mu^3 a^2 - a^2 + 3a^4 - 5\mu a^4]\left[\arctan\left[\frac{1-\mu}{a}\right] + \arctan\left[\frac{\mu}{a}\right]\right], \quad \text{(A8)}$$

which comes from the direct terms, and

$$I_2(\mu,a) = \int_0^1 dx \int_0^{1-x} dy \frac{N(y,1-x-y)y^2(1-x-y)^2}{D(y)D(1-x-y)}$$
$$= \tfrac{1}{24} + \tfrac{1}{3}\mu - \mu^2 - \mu^3 + 2a^2 - 5a^2\mu + \tfrac{1}{2}[\mu^2 - \mu^4 + 8a^2\mu - 6a^2\mu^2 - a^2 + 3a^4]\ln\left[\frac{(1-\mu)^2+a^2}{\mu^2+a^2}\right]$$
$$+ 2a(2\mu-1)(\mu+2a^2)\left[\arctan\left[\frac{1-\mu}{a}\right] + \operatorname{arctanh}\left[\frac{\mu}{a}\right]\right]$$
$$+ 2(\mu^2+a^2)\operatorname{Re}\left[\operatorname{Sp}\left[\frac{\mu+ia}{\mu^2+a^2}2\mu\right] - \operatorname{Sp}\left[\frac{\mu+ia}{\mu^2+a^2}(2\mu-1)\right]\right], \quad \text{(A9)}$$

which is from the interference terms, where Sp is the Spence function defined by

$$\operatorname{Sp}(z) = -\int_0^1 \frac{dr}{r}\ln(1-zr), \quad \text{(A10)}$$

valid for complex arguments.

If the width Γ_H is small compared to m_H and $\sqrt{s}$, the interference terms are generally small, except when $m_H^2 \ll s$, in which case $I_2 = I_1/4$. In the limit $\Gamma_H \ll m_H$, $\sqrt{s}$ and $m_H \lesssim \sqrt{s}$, I_1 reduces to $\pi m_H^3(1-m_H^2/s)^3/(2\Gamma_H s)$, which gives the same total cross section as Eq. (4.2) for a real H^0 when the branching ratio for $H^0 \to \gamma\gamma$ is included.

The acollinearity angle is defined as

$$\zeta = \arccos[\max(-\cos\theta_{12}, -\cos\theta_{13}, -\cos\theta_{23})], \quad \text{(A11)}$$

where

$$\cos\theta_{12} = \frac{xy + x + y - 1}{(1-x)(1-y)},$$
$$\cos\theta_{13} = \frac{x - y - xy - x^2}{(1-x)(x+y)}, \quad \text{(A12)}$$
$$\cos\theta_{23} = \frac{y - x - xy - y^2}{(1-y)(x+y)},$$

and θ_{ij} is the angle between photon three-momenta $\mathbf{p}_i$ and $\mathbf{p}_j$. The acollinearity distribution can be found using Eqs. (A11) and (A12) weighted with the differential cross section of Eq. (A5). In the narrow-width approximation where

$$D(x) \approx s\pi\delta(x - m_H^2/s)m_H\Gamma_H,$$

the three direct terms dominate and yield identical results for the total cross section and acollinearity distribution. This last property is a consequence of the identity of the three final-state photons. Thus the x-y phase space for the differential cross section can be reduced to the line defined by $x = m_H^2/s$, $0 \le y \le 1-x$; the distribution is flat along this line with normalization

$$\frac{d\sigma}{dy} = \frac{8\pi\alpha}{3}\frac{\Gamma_{H\to\gamma\gamma}}{m_H^3}\left[1 - \frac{m_H^2}{s}\right]^2 B(H\to\gamma\gamma). \quad \text{(A13)}$$

The acollinearity distribution shown in Fig. 4 is calculated in this manner, with $\Gamma_{H\to\gamma\gamma}/m_H^3 = 64\pi f_{H\gamma\gamma}^2$ a constant as dictated by WDM II.

There will also be interference between the pure QED $\gamma\gamma\gamma$ production and the Higgs-boson-induced $\gamma\gamma\gamma$ process. Because the QED cross section is strongly peaked when the three photons are near the beam, this interference should be small at angles away from the beam direction.

*Permanent address.

[1]S. Weinberg, Phys. Rev. Lett. **39**, 252 (1977); A. Salam, in *Elementary Particle Theory: Relativistic Groups and Analyticity* (Nobel Symposium No. 8), edited by N. Svartholm (Almqvist and Wiksell, Stockholm, 1968), p. 367.

[2]P. Langacker and H. Arthur Weldon, Phys. Rev. Lett. **52**, 1377 (1984); R. Dashen and H. Neuberger, *ibid.* **50**, 1897 (1983); N. Cabibbo, L. Maiani, G. Parisi, and R. Petronzio, Nucl. Phys. **B158**, 295 (1979); L. Maiani, G. Parisi, and R. Petronzio, *ibid.* **B136**, 115 (1978); B. W. Lee, C. Quigg, and H. B. Thacker, Phys. Rev. Lett. **38**, 883 (1977); Phys. Rev. D **16**, 1519 (1977); M. Veltman, Acta Phys. Pol. **B8**, 475 (1977); Phys. Lett. **B70**, 253 (1977); D. A. Dicus and W. S. Mathur, Phys. Rev. D **7**, 3111 (1973).

[3]A. D. Linde, Zh. Eksp. Teor. Fiz. **23**, 73 (1976) [JETP Lett. **23**, 64 (1976)]; Phys. Lett. **70B**, 306 (1977); S. Weinberg, Phys. Rev. Lett. **36**, 294 (1976).

[4]S. R. Moore, K. Whisnant, and Bing-Lin Young, Phys. Rev. D **31**, 105 (1985); and in preparation.

[5]UA1 collaboration, G. Arnison *et al.*, Phys. Lett. **122B**, 103 (1983); **126B**, 398 (1983); **129B**, 273 (1983); UA2 collaboration, M. Banner *et al.*, Phys. Lett. **122B**, 476 (1983); and P. Bagnaia *et al.*, *ibid.* **129B**, 130 (1983).

[6]L. Susskind, Phys. Rev. D **20**, 2619 (1979); K. Wilson, *ibid.* **3**, 1818 (1971); S. Weinberg, *ibid.* **19**, 1277 (1979).

[7]For a general discussion of composite Higgs bosons, see E. Farhi and L. Susskind, Phys. Rep. **74**, 277 (1981).

[8]F. M. Renard, Phys. Lett. **116B**, 296 (1982); **126B**, 59 (1983).

[9]L. Resnick, M. K. Sundaresan, and P. J. S. Watson, Phys. Rev. D **8**, 172 (1973).

[10]G. 't Hooft and M. Veltman, Nucl. Phys. **B44**, 189 (1972); C. G. Bollini and J. J. Giambiagi, Phys. Lett. **40B**, 566 (1979); J. F. Ashmore, Lett. Nuovo Cimento **4**, 289 (1972); G. M. Cicuta and E. Montaldi, *ibid.* **4**, 329 (1972).

[11]W. Pauli and F. Villars, Rev. Mod. Phys. **21**, 434 (1949); S. N. Gupta, Proc. Soc. London **A66**, 129 (1953).

[12]See, for example, L. Lewin, *Dilogarithms and Associated Functions* (Macdonald, London, 1958), Chap. 9, Secs. 2.1 and 2.5.

[13]J. Ellis, M. K. Gaillard, and D. V. Nanopoulos, Nucl. Phys. **B106**, 292 (1976).

[14]See the discussion by R. D. Peccei, *in Proceedings of the 4th Topical Workshop on Proton-Antiproton Physics,* edited by H. Hanni and J. Schacher (Report No. CERN-84-09), p. 483. See also V. Visnjic, Phys. Lett. **143B**, 158 (1984).

[15]That low-mass compositeness scales do not necessarily contradict theoretical considerations has been discussed in, e.g., Ref. 14.

[16]J. D. Bjorken, Phys. Rev. D **19**, 335 (1978).

[17]P. Q. Hung and J. J. Sakurai, Nucl. Phys. **B143**, 81 (1978).

[18]D. Schildknecht, *in Proceedings of the XIXth Rencontre de Moriond,* edited by J. Tran Thanh Van (Editions Frontieres, Gif-sur-Yvette, France, 1984), Vol. I, p. 383.

[19]H. Fritzsch, in *Unification of the Fundamental Particle Interactions—II,* proceedings of the Second Europhysics Study Conference, Erice, 1981, edited by J. Ellis and S. Ferrara (Plenum, New York, 1983); Report No. CERN-TH-3219 (unpublished).

[20]F. Wilczek, Phys. Rev. Lett. **39**, 1304 (1977).

[21]H. Primakoff, Phys. Rev. **81**, 899 (1951).

[22]S. Gasiorowicz, *Elementary Particle Physics* (Wiley, New York, 1966), Chap. 26.

[23]We used the parametrization of Ref. 22. However, notice a typographical error in Eq. (26.16).

[24]V. Barger and R. J. N. Phillips, Nucl. Phys. **B73**, 269 (1974).

[25]J. T. Dakin and G. J. Feldman, Phys. Rev. D **8**, 2862 (1972).

[26]D. E. Wood, Ph.D. thesis, Purdue University, 1984.

[27]UA1 collaboration, G. Arnison *et al.*, Phys. Lett. **135B**, 250 (1984); UA2 collaboration, P. Bagnaia *et al.*, *ibid.* **129B**, 130 (1983). See also C. Rubbia, in *Proceedings of the International Europhysics Conference on High Energy Physics, Brighton, 1983,* edited by J. Guy and C. Costain (Rutherford Appleton Laboratory, Chilton, Didcot, United Kingdom, 1983), pp. 877–879.

[28]R. Van Royan and V. F. Weisskopf, Nuovo Cimento **50A**, 617 (1967).